PROCEEDINGS of the
23rd International Congress on Acoustics

9 to 13 September 2019 in Aachen, Germany

In-situ transfer path analysis of multiple vibration sources in a complex source- receiver assembly

Lucy BARTON[1]; Andrew ELLIOTT[1]; Andy MOORHOUSE[1]; John SMITH[2]

[1] University of Salford, England

[2] DSTL, England

ABSTRACT

Depending on where the source-receiver boundary is defined within an assembly, an airborne sound source can also be considered as a structure borne sound source. For example, if the internal forcing mechanisms within a machine are regarded as the sources, the rest of the assembly including the surrounding air can be considered the receiver. If the structure borne noise resulting from these internal forcing mechanisms can be predicted in real-time, the radiated noise can potentially be predicted and managed- either actively or passively- using numerous approaches. The primary aim of the work presented in the paper is the development of an accurate method for the real-time prediction of structure borne noise, whilst continually monitoring the reliability of these predictions. To facilitate this process, it is necessary to also monitor the stability of the vibro-acoustic frequency response functions that relate the internal forcing mechanisms to the receiver position, and to eliminate the influence of background noise resulting from noise or vibration sources other than those of interest. Presented in the paper are the results of a laboratory Transfer Path Analysis (TPA) case study of a source-receiver assembly composed of multiple sources attached to a single receiver structure.

Keywords: Noise, TPA, Transmission

1. INTRODUCTION

This paper documents a case study carried out as part of a wider PhD project investigating the use of In-Situ TPA methods (1) for the prediction of radiated noise. Considering an arbitrary source and receiver structure, predictions are made for a remote response point on the receiver by using a matrix of collected FRFs from the coupling points of the source and receiver as a reference point to validate the accuracy of the predictions. The wider scope of the project aims to evaluate methods for the prediction of noise created by the structure, consisting of multiple sources, with a focus on methods which can be implemented in real time. Also considered are elements of structural health monitoring, such as unmeasured background noise, extra connection points, and source de-activation.

The paper outlines the background theory of transfer path analysis and in-situ transfer path analysis using the matrix inversion method (section 2.1) together with alternative formulations using cross spectral matrices and principal component analysis (section 2.2). Following that an experiment is described which consists of two vibration sources incorporated into an assembly and it is shown that in-situ transfer path analysis can be used to identify the contributions from each source to the overall response of the receiver structure when both sources are operating simultaneously. Finally, a fault (bridging of the vibration isolation) on one of the vibration sources is introduced and it is shown that the sum of the contributions of the two sources no longer equals that observed in the receiver structure due to the additional path. A future aim of the study is to investigate methods that not only identify the presence of a fault but also to locate its origin, i.e. which item of equipment is affected, ideally using operational data measured simultaneously on the source and receiver structures.

2. THEORY

Following is a description of the TPA approach and Principal Component Analysis. The theory is presented for a simple source- receiver structure, where one or more sources (A) are coupled to an arbitrary receiver structure (B) through multiple contacts at an interface (c). The target quantity to be predicted can be either a remote point away from the structure itself (sound pressure at d), or a remote point on the receiver (e.g. acceleration at b).

2.1 Conventional Transfer Path Analysis

The conventional matrix inversion TPA method, or source path contribution method, uses inverse force synthesis to find the operational forces at work on the interface between the vibrating source and the receiver of an assembly.

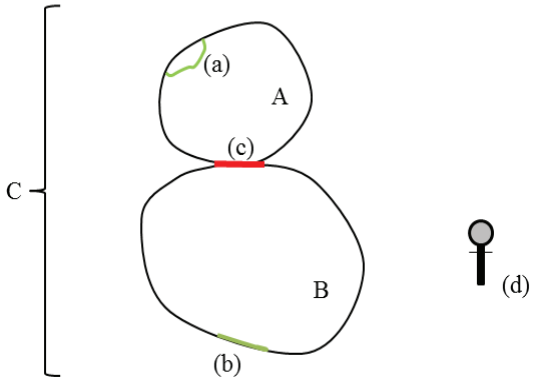

Figure 1: Schematic for source- receiver structure

Figure 1 shows a schematic diagram of an arbitrary vibration source A coupled to an arbitrary receiver structure B. The vibration source has multiple generalised forces at (a) during operation, which may then apply forces to the receiver structure B through the interface (c).

The sound pressures at position (d) are a combination of the airborne sound radiated by the source A and the structure borne sound radiated by the receiver B. The points (b) shown on subsystem B of the assembly C may be considered as a set of vibration velocities due to the internal mechanisms of A. Inverse force synthesis (2)

A set of complex operational forces, $f_{C,c}$, at interface (c) can be found using,

$$\dot{\mathbf{f}}_{\mathbf{C,c}} = \mathbf{Y}^{-\mathbf{1}}_{\mathbf{B,cc}}\dot{\mathbf{v}}_{\mathbf{C,c}} \tag{1}$$

$$\dot{\mathbf{f}}_{\mathbf{C,c}} = \mathbf{Y}^{+}_{\mathbf{B,bc}}\dot{\mathbf{v}}_{\mathbf{C,b}} \tag{2}$$

$$\dot{\mathbf{f}}_{\mathbf{C,c}} = \left[\frac{\mathbf{y}_{\mathbf{B,cc}}}{\mathbf{Y}^{\mathbf{T}}_{\mathbf{B,cb}}}\right]^{+}\left\{\frac{\dot{\mathbf{v}}_{\mathbf{C,c}}}{\dot{\mathbf{v}}_{\mathbf{C,b}}}\right\} \tag{3}$$

Where: upper-case subscripts are the structure *A, B, C*; lower case are measurement location (a), (b), (c), (d); and a dot denotes that the source is operational. $\dot{\mathbf{v}}_{\mathbf{C,c}}$ and $\dot{\mathbf{v}}_{\mathbf{C,b}}$ are the vectors of complex velocities at measurement locations (c) and (b), on assembly *C*, whilst the source A is operational. Subscripts denote row (response) then column (excitation): $\mathbf{y}_{\mathbf{B,cc}}$ and $\mathbf{y}_{\mathbf{B,bc}} = \mathbf{Y}^{\mathbf{T}}_{\mathbf{B,cb}}$ are matrices of frequency response functions of velocities due to force/ mobility (3); $\mathbf{y}_{\mathbf{B,cc}}$ is a square symmetric mobility matrix for the receiver *B*, where the rows are the responses and columns are excitations on the interface (c).

$\mathbf{y}_{\mathbf{B,bc}}$ is usually measured as $\mathbf{Y}^{\mathbf{T}}_{\mathbf{B,cb}}$. It is not symmetric and may not be square, so is pseudo-inverted. Equation 3 includes a square symmetric matrix, allowing optimization by over

determination and regularization, which is desirable due to the fact that inverting the often large FRF matrix for finding the operational forces at (c) can be highly sensitive to noise and other inconsistencies. In most cases equation 1 is sufficient and Equation 2 might be used in the case the interface (c) is not physically accessible, which can be a problem when manually exciting the structure.

The sound pressure at point (d) is then found using:

$$\dot{\mathbf{P}}_{\mathbf{C,d}} = \mathbf{H}_{\mathbf{B,dc}}\dot{\mathbf{f}}_{\mathbf{C,c}} \tag{4}$$

Where $\dot{\mathbf{P}}_{\mathbf{C,d}}$ is a complex vector of radiated sound pressures from the receiver *B*, caused by the operational source *A*. The matrix $\mathbf{H}_{\mathbf{B,dc}}$ is made up of sound pressure frequency response functions due to force, or through reciprocal measurements, velocity due to volume velocity excitation (4).

2.2 In-situ Transfer Path Analysis

In-situ transfer path analysis is an alternative to conventional TPA that does not require the source receiver-assembly to be dismantled with the use of blocked forces rather than interface forces, where the blocked force for the source *A* in Figure 2 is defined by:

$$\bar{\dot{\mathbf{f}}}_{\mathbf{A,c}} = -\dot{\mathbf{f}}_{\mathbf{A,c}}\big|_{\dot{\mathbf{v}}_{\mathbf{A,c}}=\mathbf{0}} \tag{5}$$

where the bar denotes that the force is blocked.

The mobilities of the subsystems which make up the assembly *C* provide the relationship between the operational blocked forces of the source *A* and the operational forces of the assembly *C*.

$$\dot{\mathbf{f}}_{\mathbf{C,c}} = \left(\mathbf{Y}_{\mathbf{A,cc}} + \mathbf{Y}_{\mathbf{B,cc}}\right)^{-\mathbf{1}}\mathbf{Y}_{\mathbf{A,cc}}\bar{\dot{\mathbf{f}}}_{\mathbf{A,c}} \tag{6}$$

Which after substitution and rearrangement of equations 1-3, gives the blocked force version of these equations.

$$\bar{\dot{\mathbf{f}}}_{\mathbf{A,c}} = \mathbf{Y}_{\mathbf{C,cc}}^{-\mathbf{1}}\dot{\mathbf{v}}_{\mathbf{C,c}} \tag{7}$$

$$\bar{\dot{\mathbf{f}}}_{\mathbf{A,c}} = \mathbf{Y}_{\mathbf{C,bc}}^{+}\dot{\mathbf{v}}_{\mathbf{C,b}} \tag{8}$$

$$\bar{\dot{\mathbf{f}}}_{\mathbf{A,c}} = \begin{bmatrix}\mathbf{Y}_{\mathbf{C,cc}} \\ \hline \mathbf{Y}_{\mathbf{C,bc}}^{\mathbf{T}}\end{bmatrix}^{+}\begin{Bmatrix}\dot{\mathbf{v}}_{\mathbf{C,c}} \\ \hline \dot{\mathbf{v}}_{\mathbf{C,b}}\end{Bmatrix} \tag{9}$$

Finally, assuming that the sound pressure at (d) caused by structure *A* during the measurement of *H* is negligible, the structure borne noise at (d) is:

$$\dot{\mathbf{P}}_{\mathbf{C,d}} = \mathbf{H}_{\mathbf{C,dc}}\bar{\dot{\mathbf{f}}}_{\mathbf{A,c}} \tag{10}$$

where $\mathbf{H_{C,dc}}$ is the measured transfer function for the entire assembly *C*, as opposed to $\mathbf{H_{B,dc}}$, used in equation 4, which is only for the receiver structure. Thus, the method does not require the separation of source and receiver saving time and effort. Another advantage of the in-situ approach is that the operational blocked forces are independent of the receiver structure, meaning that they remain valid for different assemblies by re-measuring or modelling $\mathbf{H_{C,dc}}$ for the new assembly. This property is not shared by the conventional approach as the contact forces measured can vary significantly between receiver structures (5).

2.3. Principal Component Analysis

When a system has multiple uncorrelated system inputs, the measured operational data is sometimes conditioned using principal component analysis to avoid issues resulting from averaging in the frequency domain (6,7). Considering the matrix inversion TPA approach outlined in section 2.1, figure 1 shows the interfaces of a coupled system. If there are multiple uncorrelated operational forces (vibration source mechanisms) acting at the (a), the velocities at (c) may not be fully correlated, meaning there may not be a steady phase relationship between the (c) positions. The relative phases of the forces at (c) must be known to ensure the phase information is correct for the partial pressure contribution predictions (1). By referencing the operational data to virtual sources, or principle components, PCA aims to alleviate this issue.
As opposed to the vector form of complex operational data shown in the matrix inversion method, PCA uses a cross spectral matrix, for which a definition for the sets of points and degrees of freedom on interface (c) is shown by:

$$\dot{\mathbf{G}}_{\mathbf{C,cc}} = \mathbf{E}\left[\dot{\mathbf{v}}_{\mathbf{C,c}}\dot{\mathbf{v}}_{\mathbf{C,c}}^{\mathbf{H}}\right] \tag{11}$$

Where $\dot{\mathbf{G}}$ is the averaged cross spectral matrix of the velocities, $\dot{\mathbf{v}}_{\mathbf{C,c}}$ is instantaneous velocity vector, *E* denotes 'expectation of', and *H* is the Hermitian transpose. Equations 1-3 and 7-9 can all be converted to this form by post-multiplying both sides by its own complex conjugate transpose. For example, equation 1 $\dot{\mathbf{f}}_{\mathbf{C,c}} = \mathbf{Y}_{\mathbf{B,cc}}^{-\mathbf{1}}\dot{\mathbf{v}}_{\mathbf{C,c}}$ becomes:

$$\dot{\mathbf{F}}_{\mathbf{C,cc}} = \mathbf{Y}_{\mathbf{B,cc}}^{-\mathbf{1}}\dot{\mathbf{G}}_{\mathbf{C,cc}}\mathbf{Y}_{\mathbf{B,cc}}^{-\mathbf{H}} \tag{12}$$

And equation 7 $\dot{\bar{\mathbf{f}}}_{\mathbf{A,c}} = \mathbf{Y}_{\mathbf{C,cc}}^{-\mathbf{1}}\dot{\mathbf{v}}_{\mathbf{C,c}}$ becomes:

$$\dot{\bar{\mathbf{F}}}_{\mathbf{A,cc}} = \mathbf{Y}_{\mathbf{B,cc}}^{-\mathbf{1}}\dot{\mathbf{G}}_{\mathbf{C,cc}}\mathbf{Y}_{\mathbf{B,cc}}^{-\mathbf{H}} \tag{13}$$

Where $\dot{\bar{\mathbf{F}}}$ is the force cross spectral matrix, instead of f (force vector). Equation 4 $\dot{\mathbf{P}}_{\mathbf{C,d}} = \mathbf{H}_{\mathbf{B,dc}}\dot{\mathbf{f}}_{\mathbf{C,c}}$ now becomes:

$$\dot{\mathbf{G}}_{\mathbf{C,dd}} = \mathbf{H}_{\mathbf{B,dc}}\dot{\mathbf{F}}_{\mathbf{C,cc}}\mathbf{H}_{\mathbf{B,dc}}^{\mathbf{H}} \tag{14}$$

And equation 10 $\dot{\mathbf{P}}_{\mathbf{C,d}} = \mathbf{H}_{\mathbf{C,dc}}\dot{\bar{\mathbf{f}}}_{\mathbf{A,c}}$ becomes:

$$\dot{\mathbf{G}}_{\mathbf{C,dd}} = \mathbf{H}_{\mathbf{B,dc}}\dot{\bar{\mathbf{F}}}_{\mathbf{A,cc}}\mathbf{H}_{\mathbf{C,dc}}^{\mathbf{H}} \tag{15}$$

Here, $\dot{\mathbf{G}}_{\mathbf{C,dd}}$ is a cross-spectral matrix of sound pressure at (d) - the auto-spectra are on the diagonal. A principle component analysis can now be conducted using a set of slave/ reference sensors for determination of the 'virtual sources'. If these sensors are placed at (a), the cross-spectral matrix $\dot{\mathbf{G}}_{\mathbf{C,aa}} = \mathbf{E}\left[\dot{\mathbf{v}}_{\mathbf{C,a}}\dot{\mathbf{v}}_{\mathbf{C,a}}^{\mathbf{H}}\right]$ of size $n \times n$ is defined (where n is the number of sensors at (a)). The auto-spectra of the principle components can then be found from the eigenvalue or singular value decomposition

of the reference cross spectral matrix:

$$\dot{\mathbf{G}}_{\mathbf{C,aa}} = \mathbf{E}\left[\dot{\mathbf{v}}_{\mathbf{C,a}}\dot{\mathbf{v}}_{\mathbf{C,a}}^{\mathbf{H}}\right] = \mathbf{U}\dot{\mathbf{S}}_{\mathbf{C,aa}}\mathbf{U}^{\mathbf{H}} \tag{16}$$

$\mathbf{U}$ is a unitary matrix and the singular values $\dot{\mathbf{S}}_{\mathbf{C,aa}}$ are the principle components. Velocity spectra referenced to the principle components (6) are then found for the degrees of freedom at (c) and (b) using:

$$\begin{bmatrix}\dot{\mathbf{v}}'_{\mathbf{C,c}}\\ \dot{\mathbf{v}}'_{\mathbf{C,b}}\end{bmatrix} = \begin{bmatrix}\dot{\mathbf{G}}_{\mathbf{C,ac}}\\ \dot{\mathbf{G}}_{\mathbf{C,bc}}\end{bmatrix}[\mathbf{U}]\left[\dot{\mathbf{S}}_{\mathbf{C,aa}}\right]^{-1/2} \tag{17}$$

Where $\dot{\mathbf{v}}'_{\mathbf{C,c}}$ are the referenced velocity spectra with rows relating to the velocities at (c), $\dot{\mathbf{v}}'_{\mathbf{C,b}}$ are the referenced velocity spectra with rows relating to the velocities at (b) and the columns of each are referenced to principle components according to the references at (a). The reference spectra $\dot{\mathbf{P}}'_{\mathbf{C,d}}$ can be converted from the sound pressures at (d) using:

$$\left[\dot{\mathbf{P}}'_{\mathbf{C,d}}\right] = \left[\dot{\mathbf{G}}_{\mathbf{C,ad}}\right][\mathbf{U}]\left[\dot{\mathbf{S}}_{\mathbf{C,aa}}\right]^{-1/2} \tag{18}$$

The matrix inversion method can then be conducted using the referenced spectra in (7.7) to find a partial pressure contribution prediction for each position of (d), with reference to a virtual source. The conventional method would take the form:

$$\left[\dot{\mathbf{P}}'_{\mathbf{C,d}}\right] = \mathbf{H}_{\mathbf{B,dc}}\begin{bmatrix}\mathbf{Y}_{\mathbf{B,cc}}\\ \mathbf{Y}_{\mathbf{B,cb}}^{\mathbf{T}}\end{bmatrix}^{+}\begin{bmatrix}\dot{\mathbf{v}}'_{\mathbf{C,c}}\\ \dot{\mathbf{v}}'_{\mathbf{C,b}}\end{bmatrix} \tag{19}$$

With the in-situ method taking the form:

$$\left[\dot{\mathbf{P}}'_{\mathbf{C,d}}\right] = \mathbf{H}_{\mathbf{C,dc}}\begin{bmatrix}\mathbf{Y}_{\mathbf{C,cc}}\\ \mathbf{Y}_{\mathbf{C,cb}}^{\mathbf{T}}\end{bmatrix}^{+}\begin{bmatrix}\dot{\mathbf{v}}'_{\mathbf{C,c}}\\ \dot{\mathbf{v}}'_{\mathbf{C,b}}\end{bmatrix} \tag{20}$$

Where equation 17 is used to obtain $\begin{bmatrix}\dot{\mathbf{v}}'_{\mathbf{C,c}}\\ \dot{\mathbf{v}}'_{\mathbf{C,b}}\end{bmatrix}$ (1).

3. EXPERIMENT

The experiment was carried out on a bespoke test rig, consisting of an aluminium box with a steel 'lid' plate. Two smaller rafts are attached to the lid via vibration isolators, with one isolator at the corner of each raft.

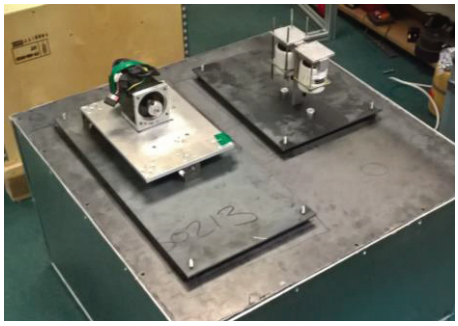

Figure 2: Test Rig

In order to test as many positions as possible, the testing was carried out in stages. Firstly, the motor was placed in situ and the coupling points were instrumented with six accelerometers each in order to obtain accelerations in 5 degrees of freedom (three translations and two rotations). To create a better surface for impacts, the accelerometers were mounted on blocks at each coupling point. FRF's for five degrees of freedom at each coupling point were then obtained using an instrumeted

hammer. A triaxial was mounted on the motor itself as a phase reference during operational measurements.

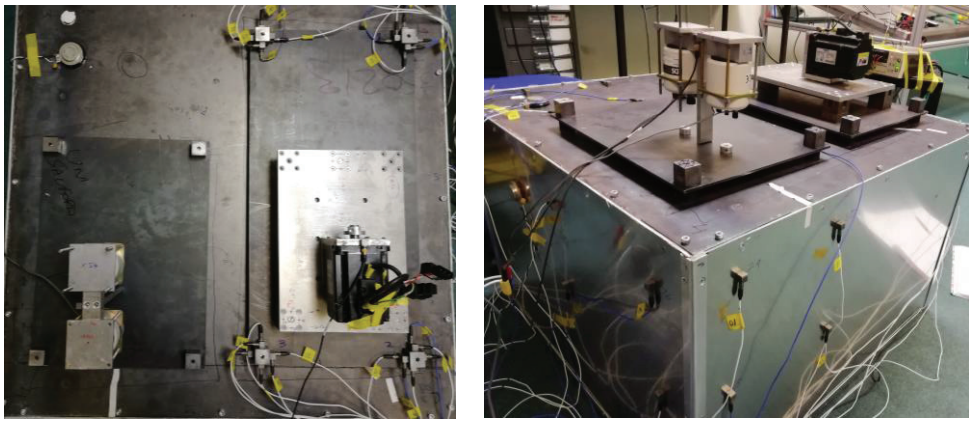

Figure 3&4: Motor test and receiver test

Following the FRF measurements, testing with motor running was conducted. The motor was run at speeds of 2kHz, 3kHz, and 4kHz.

The accelerometers were then transferred to the shaker coupling points and the testing repeated. The accelerometers were then moved to twenty-one remoted positions on the receiver box, with a triaxial accelerometer on each of the sources.

4. RESULTS

Equation 13 $\dot{\bar{\mathbf{F}}}_{\mathbf{A,cc}} = \mathbf{Y}_{\mathbf{B,cc}}^{-\mathbf{1}}\dot{\mathbf{G}}_{\mathbf{C,cc}}\mathbf{Y}_{\mathbf{B,cc}}^{-\mathbf{H}}$, was used to determine the forces required as the input to Equation 14, $\dot{\mathbf{G}}_{\mathbf{C,dd}} = \mathbf{H}_{\mathbf{B,dc}}\dot{\mathbf{F}}_{\mathbf{C,cc}}\mathbf{H}_{\mathbf{B,dc}}^{\mathbf{H}}$, Where H is a set of transfer FRF's relating the source receiver coupling points to the response point on the box. These values were calculated for both the shaker and motor, as seen in the lower plot of figure 5.

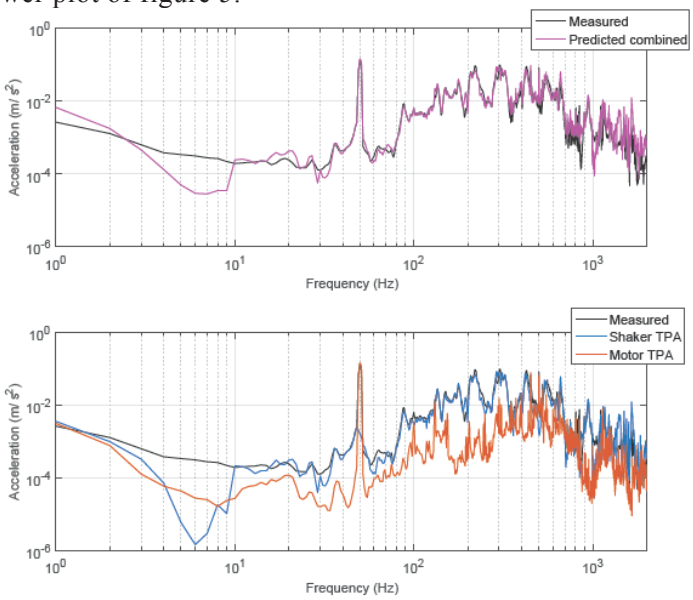

Figure 5: Plot of predictions using Equations 14 and 15 (motor 4kHz speed)

This plot shows the individual contributions of source to the overall measured vibration level. It can be observed that the shaker contributes most of the broadband signal, whereas the tonal peak at ~500Hz is contributed by the motor. The upper plot shows the two predictions added together to make an overall combined prediction. Good agreement is observed at this operational speed (4kHz).

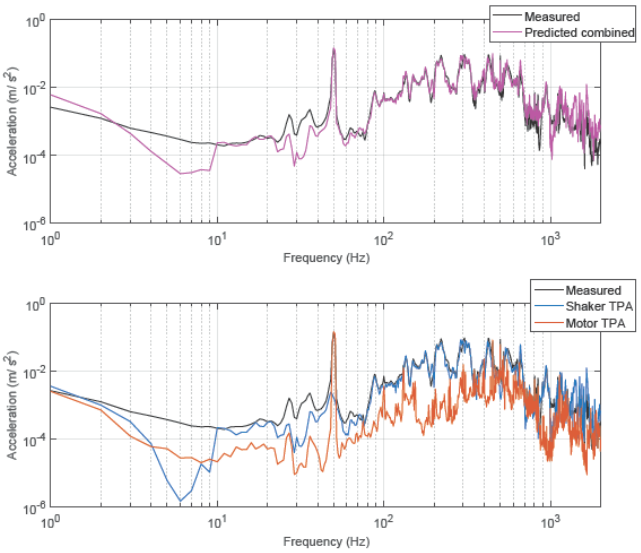

Figure 6: (motor 3kHz)

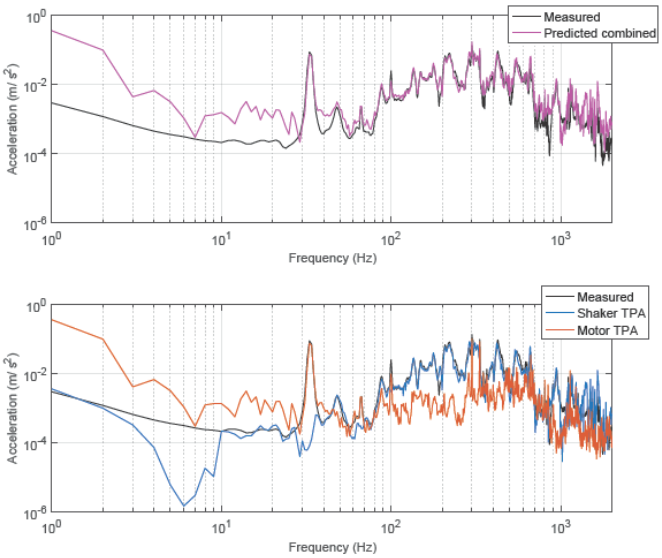

Figure 7: (motor 2kHz)

Figures 6&7 show that the prediction works for the varying speeds of motor; the peaks in the measured response and in the calculated prediction appear to have very good agreement, and are accurate from ~20Hz, up to approximately 1kHz. This restriction may be due to the degrees of freedom used. A more detailed instrumentation of the coupling points may lead to better accuracy at higher frequencies. The frequency range is also dependent on the accelerometers used and the level of vibration isolation provided by the vibration isolators under each raft structure; for example, accelerometers with a higher sensitivity could potentially give better predictions at both ends of the frequency range shown.

5. FAULT CONDITION

As mentioned in the introduction one of the aims of the project is to identify system faults using the measured operational data in real time. For this reason a known fault was introduced to the source receiver assembly by bridging the isolation system on one of the sources.
The introduced fault condition consisted of a small magnetic structure which created a bridge between the motor raft and the lid of the box, which created an unaccounted connection point between the source and the receiver.

Figure 8: Fault condition

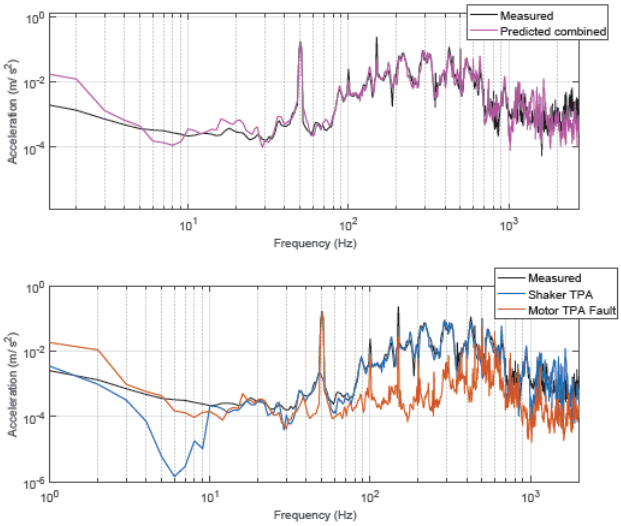

Figure 9: Fault condition results (motor 4kHz)

The upper plot of Figure 9 shows the measured response against the calculated response, as shown in Figures 5. It can be seen that additional tones are now present in the receiver response. The lower plot shows the individual contributions of each source. The motor measurement corresponds to these additional tones in the overall response, but the overall level calculated from the blocked forces of the two sources is now no longer in agreement at these frequencies, highlighting the presence of the fault.

6. Conclusions

In conclusion, the contributions from each source have been accurately identified with simultaneous source operation using cross-spectral matrices. It is also shown that following the introduction of a fault, the sum of the contributing sources no longer corresponds completely with the observed vibration. The next stages implied are to further investigate the possibilities of source separation using the PCA methods described, and to carry these out in the presence of background noise.

REFERENCES

1. Elliott AS, Moorhouse AT, Huntley T, Tate S. In-situ source path contribution analysis of structure borne road noise. J Sound Vib. 2013;
2. Dobson BJ, Rider E. A Review of the Indirect Calculation of Excitation Forces from Measured Structural Response Data. Proceedings of the Institution of Mechanical Engineers, Part C: Journal of Mechanical Engineering Science. 1990.
3. Ewins DJ. Modal testing : theory, practice, and application. 2nd ed. Philadelphia, PA: Research Studies Press, Baldock, Hertfordshire, England; 2000.
4. Verheij JW. Inverse and Reciprocity Methods for Machinery Noise Source Characterization and Sound Path Quantification Part 1: Sources. Int J Acoust Vib [Internet]. 1997;2(1):11–20. Available from: http://s3.amazonaws.com/academia.edu.documents/38269668/Jan_Verheij_-Inverse_and_Reciprocity_Methods_for_Machinery_Noise_-_Part_1_Sources.pdf?AWSAccessKeyId=AKIAIWOWYYGZ2Y53UL3A&Expires=1494226668&Signature=nopyeQWx1toaVcDhxLgfPDXQ5L4%3D&response-content-
5. Elliott A. Characterisation Of Structure Borne Sound Sources In-Situ. PhD Thesis. University Of Salford, Greater Manchester; 2009.
6. D. Hendricx WSFV. Interior road noise optimization in a multiple input environment. Inst Mech Eng Conf Publ 3. 1994;3:53–8.
7. Otte, D. Development and Evaluation of Singular Value Analysis Methodologies for Studying Multivariate Noise and Vibration Problems [Internet]. PhD K. U. Leuven. 1994 [cited 2018 Aug 23]. Available from: https://ci.nii.ac.jp/naid/10003083914/